Inorg. Chem. **2007**, *46*, 825–838

Electroactive Thiazole Derivatives Capped with Ferrocenyl Units Showing Charge-Transfer Transition and Selective Ion-Sensing Properties: A Combined Experimental and Theoretical Study

Antonio Caballero,[†] Vega Lloveras,[‡] David Curiel,[†] Alberto Tárraga,[†] Arturo Espinosa,[†] Rafaela García,[†] José Vidal-Gancedo,[‡] Concepció Rovira,[‡] Klaus Wurst,[§] Pedro Molina,*[,†] and Jaume Veciana*[,‡]

Departamento de Química Orgánica, Facultad de Química, Campus de Espinardo, Universidad de Murcia, E-30100 Murcia, Spain, Institut de Ciència de Materials de Barcelona (CSIC), Campus Universitari de Bellaterra, E-08193 Cerdanyola, Spain, and Institut für Allgemeine Anorganische und Teoretische Chemie, Universität Innsbrück, Innrain 52a, A-6020 Innsbruck, Austria

Received September 22, 2006

The synthesis, optical and electrochemical properties, and X-ray characterization of two thiazole derivatives capped by ferrocenyl groups (**5** and **7**) and their model compounds with one ferrocenyl, either at 2 or 5 position of the mono- or bis-thiazolyl rings (**3**, **9**, **11**, and **14**), are presented. Bisferrocenyl thiazole **5** forms the mixed-valence species $\mathbf{5}^{\bullet+}$ by partial oxidation which, interestingly, shows an intramolecular electron-transfer phenomenon. Moreover, the reported heteroaromatic compounds show selective ion-sensing properties. Thus, ferrocenylthiazoles linked across the 5 position of the heteroaromatic ring are selective chemosensors for Hg^{2+} and Pb^{2+} metal ions; 5-ferrocenylthiazole **3** operates through two channels, optical and redox, for Hg^{2+} and only optical for Pb^{2+}, whereas 1,1′-bis(thiazolyl)ferrocene **14** is only an optical sensor for both metal ions. Moreover, complex **3** behaves as an electrochemically induced switchable chemosensor because of the low metal-ion affinity of the oxidized $\mathbf{3}^{\bullet+}$ species. On the other hand, ferrocenylthiazole **9**, in which the heterocyclic ring and the ferrocene group are linked across the 2 position, is a selective redox sensor for Hg^{2+} metal ions, and it responds optically, as does bis(thiazolyl)-ferrocene **11**, to a narrow range of cations (Zn^{2+}, Cd^{2+}, Hg^{2+}, Ni^{2+}, and Pb^{2+}). Finally, bis(ferrocenyl)thiazole **5** is a dual optical and redox sensor for Zn^{2+}, Cd^{2+}, Hg^{2+}, Ni^{2+}, and Pb^{2+}, whereas bis(ferrocenyl) compound **7**, bearing a bis(thiazole) unit as a bridge, is only a chromogenic sensor for Zn^{2+}, Cd^{2+}, Hg^{2+}, Ni^{2+}, and Pb^{2+}. The experimental data and conclusions about both the electronic and ion-sensing properties are supported by DFT calculations which show, in addition, an unprecedented intramolecular electron-transfer reorganization after the first one-electron oxidation of compound **5**.

Introduction

Mixed-valence (MV) compounds can be regarded as the simplest models for testing electron-transfer systems.[1,2] Analysis of their intervalence charge-transfer (IVCT) transitions by the Hush theory, which links optically induced electron transfer with the Marcus theory of thermally induced electron transfer,[3] has been of considerable interest to both chemists and biologists. Complexes featuring equivalent redox-active ferrocene groups as end-caps in a molecular array represent one of the most widely investigated families of MV systems. Generally, IVCT transitions are observed when the two ferrocenes are joined either by linear π-conjugated carbon-chain bridges,[4] or metal-containing fragments,[5] although weak IVCT transitions have also been observed in a few saturated systems.[6] However, heteroaro-

* To whom correspondence should be addressed. E-mail: vecianaj@icmab.es (J.V.), pmolina@um.es (P.M.).
[†] Universidad de Murcia.
[‡] Institut de Ciència de Materials de Barcelona (CSIC).
[§] Universität Innsbrück.

(1) Robin, M. B.; Day, P. *Adv. Inorg. Chem. Radiochem.* **1967**, *10*, 247−422.
(2) Allen, G. C.; Hush, N. S. *Prog. Inorg. Chem.* **1967**, *8*, 357−389.
(3) (a) Hush, N. S. *Prog. Inorg. Chem.* **1967**, *8*, 391−444. (b) Hush, N. S. *Coord. Chem. Rev.* **1985**, *64*, 135−157.
(4) Barlow, S.; O'Hare, D. *Chem. Rev.* **1997**, *97*, 637−669 and references therein.

10.1021/ic061803b CCC: $37.00
Published on Web 01/11/2007

matic ring systems[7] capped by ferrocenyl groups are rare, and moreover, in all the reported cases the heterocyclic spacers do not allow significant electronic communication between the two ferrocene units.

We have recently reported[8] that bishomometallic complexes containing two ferrocene units linked by the electroactive 2-aza-1,3-butadiene bridge allow the study of the influence of this disymmetric bridge on the intramolecular electron-transfer (IET) phenomenon, demonstrating that this oxidizable bridge promotes the IET between the two metallic centers through two different pathways. On the basis of this body of work, we have decided to study the electrochemical and optical behavior of ferrocene derivatives linked to an electron-accepting thiazole ring as a core π-electron system, which can be viewed structurally as a 2-aza-1,3-butadiene closed by a sulfur atom. The π-bond order, calculated either by HMO or by CNDO/2 methods, is indicative of a thiazole molecule situated between an aromatic ring and a diene system, and therefore, a significant electronic communication was expected for such a system. On the other hand, in this kind of molecule, the nitrogen and sulfur atoms in the thiazole ring add another interesting and useful function such as the ability to act as metal-ion ligands. Moreover, the reversibility of the ferrocene/ferrocenium redox couple and the ability of the thiazole ring to act as a ligand toward metal ions may operate cooperatively within the molecule. This synergistic relation may create a molecular switch which would allow the complexing ability of the thiazole subcomponent to be turned off when a positive charge within the ferrocene moiety is generated. Upon reduction, complexing ability would be restored, and consequently, the combination of ferrocenes and thiazole rings could be of interest for the construction of heterobimetallic systems which can behave not only as suitable models to study the intramolecular charge-transfer across this heteroaromatic ring system but also as redox-switching receptors, via electrochemical and/or optical methodologies, with the capability of selectively sensing metal-ion guests.[9]

Experimental Section

General Procedures. All reactions were carried out using solvents which were dried by routine procedures. All melting points were determined on a hot-plate melting point apparatus and are uncorrected. IR spectra were determined as Nujol emulsions or films. ^{1}H and ^{13}C NMR spectra were recorded at 200 or 300 MHz. The following abbreviations for stating the multiplicity of the signals have been used: s (singlet), bs (broad singlet), d (doublet), t (triplet), bt (broad triplet), st (pseudotriplet), m (multiplet), and q (quaternary carbon atom). Chemical shifts refer to signals of tetramethylsilane in the case of ^{1}H and ^{13}C NMR spectra. EPR spectra were obtained with a Bruker 300 spectrometer equipped with a TE_{102} microwave cavity, a variable temperature unit, and a field frequency lock system, and line positions were determined with a NMR gaussmeter. The modulation amplitude was kept well below the line width, and the microwave power was well below saturation. Crystallographic measurements were made at 233(2) K on a diffractometer with the area detector positioned at the window of a rotating anode generator using Mo Kα radiation (0.71073 Å). The cyclic voltammetric measurements were performed on a potentiostat/galvanostat controlled by a personal computer and driven by dedicated software with a conventional three-electrode configuration consisting of platinum working and auxiliary electrodes and an SCE reference electrode. The experiments were carried out with a 10^{-3} M solution of sample in dry CH_2Cl_2 containing 0.1 M $[(n\text{-}Bu)_4N]ClO_4$ (***Warning:*** *Caution! Potential formation of highly explosive perchlorate salts of organic derivatives*) as supporting electrolyte. Deoxygenation of the solutions was achieved by bubbling nitrogen for at least 10 min, and the working electrode was cleaned after each run. The cyclic voltammograms were recorded with a scan rate between 0.05 and 0.5 V s^{-1}. The DPV voltammograms were recorded before and after the addition of aliquots of 0.1 equiv of 2.5×10^{-2} M solutions of $HBF_4 \cdot Et_2O$ in CH_3CN. The following

(5) (a) Albinati, A.; Biani, F. F.; Leoni, P.; Marchetti, L.; Pasquali, M.; Rizzato, S.; Zanello, P. *Angew. Chem., Int. Ed.* **2005**, *44*, 5701−5705. (b) Xu, G. L.; Crutchley, R. J.; DeRosa, M. C.; Pan, Q.-J.; Zhang, H.-X.; Wang, X.; Ren, T. *J. Am. Chem. Soc.* **2005**, *127*, 13354−13363 and references therein.

(6) (a) Barlow, S. *Inorg. Chem.* **2001**, *40*, 7047−7053. (b) Jones, S. C.; Barlow, S.; O'Hare, D. *Chem. Eur. J.* **2005**, *11*, 4473−4481. (c) López, J. L.; Tárraga, A.; Espinosa, A.; Velasco, M. D.; Molina, P.; Lloveras, V.; Vidal-Gancedo, J.; Rovira, C.; Veciana, J.; Evans, D. J.; Wurst, K. *Chem. Eur. J.* **2004**, *10*, 1815−1826.

(7) (a) Thomas, K. R. J.; Lin, J. T.; Wen, Y. S. *J. Organomet. Chem.* **1999**, *575*, 301−309. (b) Thomas, K. R. J.; Lin, J. T.; Lin, K. J. *Organometallics* **1999**, *18*, 5285−5291. (c) Thomas, K. R. J.; Lin, J. T.; Wen, Y. S. *Organometallics* **2000**, *19*, 1008−1012. (d) Tárraga, A.; Molina, P.; Curiel, D.; Velasco, M. D. *Organometallics* **2001**, *20*, 2145−2152. (e) Tárraga, A.; Molina, P.; Curiel, D.; Velasco, M. D. *Tetrahedron* **2001**, *57*, 6765−6774.

(8) (a) Lloveras, V.; Caballero, A.; Tárraga, A.; Velasco, M. D.; Espinosa, A.; Wurst, K.; Evans, D. J.; Vidal-Gancedo, J.; Rovira, C.; Molina, P.; Veciana, J. *Eur. J. Inorg. Chem.* **2005**, 2436−2450. (b) Caballero, A.; Tárraga, A.; Velasco, M. D.; Espinosa, A.; Molina, P. *Org. Lett.* **2005**, *7*, 3171−3174. (c) Caballero, A.; Lloveras, V.; Tárraga, A.; Espinosa, A.; Velasco, M. D.; Vidal-Gancedo, J.; Rovira, C.; Wurst, R.; Molina, P.; Veciana, J. *Angew. Chem., Int. Ed.* **2005**, *44*, 1977−1981.

(9) For reviews see: (a) Constable, E. C. *Angew. Chem., Int. Ed. Engl.* **1991**, *30*, 407−408. (b) Beer, P. D. *Adv. Inorg. Chem.* **1992**, *39*, 79−157. For specific sensors for mercury, see: (c) Brümmer, O.; La Clair, J. L.; Janda, K. D. *Org. Lett.* **1999**, *3*, 415−418. (d) Brümmer, O.; La Clair, J. L.; Janda, K. D. *Biorg. Med. Chem.* **2001**, *9*, 1067−1071. (e) Sancenón, F.; Martinez-Mañez, R.; Soto, J. *Tetrahedron Lett.* **2001**, *42*, 4321−4323. (f) Sancenón, F.; Martinez-Mañez, R.; Soto, J. *Chem. Commun.* **2001**, 2262−2263. (g) Choi, M. J.; Kim, M. Y.; Chang, S.-K. *Chem. Commun.* **2001**, 1664−1665. (h) Nolan, E. M.; Lippard, S. J. *J. Am. Chem. Soc.* **2003**, *125*, 14270−14271. (i) Descalzo, A. B.; Martinez-Mañez, R.; Radeglia, R.; Rurack, K.; Soto, J. *J. Am. Chem. Soc.* **2003**, *125*, 3418−3419. (j) Guo, X.; Qian, X.; Jia, L. *J. Am. Chem. Soc.* **2004**, *126*, 2272−2273. (k) Ros-Lis, J. V.; Martinez-Mañez, R.; Rurack, K.; Sancenon, F.; Soto, J.; Spieles, M. *Inorg. Chem.* **2004**, *43*, 5183−5185. (l) Ono, A.; Togashi, H. *Angew. Chem., Int. Ed.* **2004**, *43*, 4300−4302. (m) Moon, S. Y.; Cha, N. R.; Kim, Y. H.; Chang, S.-K. *J. Org. Chem.* **2004**, *69*, 181−183. (n) Kim, I.-B.; Erdogan, B.; Wilson, J. N.; Bunz, U. H. F. *Chem. Eur. J.* **2004**, *10*, 6247−6254. (o) Chen, Q.-Y.; Chen, C.-F. *Tetrahedron Lett.* **2005**, *46*, 165−168. (p) Youn, N. J.; Chang, S.-K. *Tetrahedron Lett.* **2005**, *46*, 125−129. (q) Moon, S.-Y.; Youn, N. J.; Park, S. M.; Chang, S.-K. *J. Org. Chem.* **2005**, *70*, 2394−2397. (r) Miyake, Y.; Ono, A. *Tetrahedron Lett.* **2005**, *46*, 2441−2443. (s) Caballero, A.; Martínez, R.; Lloveras, V.; Ratera, I.; Vidal-Gancedo, J.; Wurst, K.; Tárraga, A.; Molina, P.; Veciana, J. *J. Am. Chem. Soc.* **2005**, *127*, 15666−15667. (t) Coronado, E.; Galán-Mascarós, J. R.; Martí-Gastaldo, C.; Palomares, E.; Durrant, J.; Vilar, R.; Gratzel, M.; Nazeeruddin, M. K. *J. Am. Chem. Soc.* **2005**, *127*, 12351−12356. (u) Matsushita, M.; Meijler, M. M.; Wirsching, P.; Lerner, R. A.; Janda, K. D. *Org. Lett.* **2005**, *7*, 4943−4946. (v) Martínez, R.; Espinosa, A.; Tárraga, A.; Molina, P. *Org. Lett.* **2005**, *7*, 5869−5872. (w) Fan, L.-J.; Zhang, Y.; Jones, W. E. *Macromolecules* **2005**, *38*, 2844−2849. (x) Nolan, E. M.; Racine, M. E.; Lippard, S. J. *Inorg. Chem.* **2006**, *45*, 2742−2749. (y) Wu, Z.; Zhang, Y.; Ma, J. S.; Yang, G. *Inorg. Chem.* **2006**, *45*, 3140−3142. (z) Wang, J.; Qian, X. *Org. Lett.* **2006**, *8*, 3721−3724. (aa) Tatay, S.; Gaviña, P.; Coronado, E.; Palomares, E. *Org. Lett.* **2006**, *8*, 3858−3860.

settings were used: pulse amplitude, 50 mV; pulse width, 50 ms; scan rate, 100 mV/s; sample width, 17 ms; pulse period, 200 ms. Decamethylferrocene (DMFe) (−0.07 V vs SCE) was used as an internal reference both for potential calibration and for reversibility criteria. Oxidations were performed by electrolysis in a three-electrode cell under argon using dry CH_2Cl_2 as a solvent and 0.15 M $[(n\text{-}Bu)_4N]PF_6$ as supporting electrolyte. The progress of the oxidation was followed coulombimetrically (or chronoamperometrically) by 263A of EG&PAR potentiostat−galvanostat. The reference electrode and the counter electrode were separately immersed in the solvent containing the supporting electrolyte and isolated from the bulk solution by a glass frit. The working electrode was a platinum grid. UV−vis−near-IR absorption spectra were regularly recorded by transferring a small aliquot of the solution contained in the electrochemical cell into a UV quartz cell for different average number of removed electrons.

X-ray Measurement and Structure Determination. Data collection was performed on a Nonius Kappa CCD equipped with graphite-monochromatized Mo Kα radiation ($\lambda = 0.71073$ Å) and nominal crystals to area detector distance of 36 mm. Intensities were integrated using DENZO and scaled with SCALEPACK. Several scans in ϕ and ω direction were made to increase the number of redundant reflections, which were averaged in the refinement cycles. This procedure replaces in a good approximation an empirical absorption correction. The structures were solved with direct methods SHELXS86 and refined against F^2 SHELX97. All non-hydrogen atoms were refined with anisotropic displacement parameters. Hydrogen atoms attached to carbon atoms were calculated and refined with isotropic displacement parameters 1.2 times higher than the value of their carbon atoms. A 1:1 disorder occurs for **5** at position N1 and C2, whereas each position is occupied by half nitrogen and carbon atom. Hydrogen atoms, attached to these positions, were refined with occupancy of 0.5. The disorder can be recognized by the abnormal behavior of the thermal ellipsoids. Refinement of each disordered position alternate with a complete nitrogen atom or C−H group increase the R1-value from 0.0268 to 0.0294 or 0.0296, and the thermal ellipsoids for the nitrogen atoms are around 1.5 times higher in each direction as for three ordered atoms of the five-membered ring. Alternatively, the disorder can be seen by refinement of the disordered model without the hydrogen atoms at the disordered positions. The rest of the electron density shows two strong peaks with nearly the same electron density at the former hydrogen positions. All the crystal structures described in this article have been deposited at the Cambridge Crystallographic Data Center and allocated the deposition numbers CCDC 612848−612851. These data can be obtained free of charge from The Cambridge Crystallographic Data Center via www.ccdc.cam.ac.uk/data_request/cif.

Computational Procedures. Calculated geometries of compounds **3**, **5**, **7**, **9**, and **15**, and their oxidized counterparts, were fully optimized with the Gaussian 03[10] package at the DFT level of theory by using the B3LYP functional[11] (Becke's three parameters hybrid functional[12] with the Lee−Yang−Parr correlation functional[13]) and the 6-31G* basis set, with tight convergence criteria. Energy data were computed as SP (single-point) calculations at the B3LYP/6-311G** level. Reported total electronic energies are uncorrected for the ZPVE (zero point vibrational energy) and computed in the gas phase. Atomic charges were obtained from SP calculations at the B3LYP/6-311G** level in terms of the natural atomic orbital (NAO) basis set, by using the natural bond orbital (NBO) method. All complexation studies were carried out with all structures being fully optimized using the B3LYP functional and two different basis sets, 6-31+G* for all atoms, and 6-311G* for Mg^{2+}, Ni^{2+}, and Zn^{2+}, Stuttgart RSC-ECP[14] for Cd^{2+} and Hg^{2+}, and aug-cc-pV5Z-PP-ECP[14] for Pb (method A); 6-31G* for all atoms, but including diffuse functions for N, S, and Fe (denoted as aug-6-31G*), and using Lanl2DZ-ECP for Mg^{2+}, Ni^{2+}, Zn^{2+}, Cd^{2+}, Hg^{2+}, and Pb^{2+} (method B). Complexation energies were computed from SPE calculations at the B3LYP/6-311+G** level except for the divalent metal cations for which the same basis sets used in the optimization step were employed. Solvent (dichloromethane) effects were obtained by reaction field SP calculations on the gas-phase optimized geometries, using Cossi and Barone's CPCM (conductor-like polarizable continuum model) formalism[15] and correcting the radius for Ni^{2+}, Zn^{2+}, Cd^{2+}, Hg^{2+}, and Pb^{2+} to 1.406, 1.523, 1.720, 1.732, and 1.709 Å (i.e., increasing the implemented radius of magnesium, by the r^{cov}_M/r^{cov}_{Mg} ratio), respectively.

General Procedure for the Preparation of β-Ketoamides. To a suspension of the desired α-aminocarbonyl hydrochloride compound (1.5 mmol), in dry THF (15 mL), at room temperature and under nitrogen atmosphere, was added dry triethylamine (3.5 mmol). After the mixture was stirred for 5 min, the appropriate amount of the adequate acid chloride in dry THF (5 mL) was added, and the resulting solution was stirred at room temperature for 4−6 h. The solvent was removed by rotary evaporation, and the residue was purified by column chromatography on silica gel, eluting with the appropriate solvent to afford the corresponding β-ketoamide which was crystallized from CH_2Cl_2/Et_2O (1/1).

***N*-(Ferrocenecarbonylmethyl)benzamide (2).[16]** Yield 68%; mp 145−147 °C; $R_f = 0.58$ (CH_2Cl_2/AcOEt/*n*-Hex, 1/1/1). ^{1}H NMR (300 MHz, $CDCl_3$): δ 4.25 (s, 5H), 4.61 (s, 2H), 4.67 (d, 2H, J(H,H) = 4.05 Hz), 4.91 (s, 2H), 7.26 (bs, 1H), 7.46−7.50 (m, 3H), 7.87−7.91 (m, 2H). Anal. Calcd for $C_{19}H_{17}FeNO_2$: C, 65.73; H, 4.94; N, 4.03. Found: C, 65.95; H, 4.68; N 4.09.

***N*-(Ferrocenecarbonylmethyl)ferrocenecarboxamide (4).[16]** Yield 49%; mp 211−214 °C (d); $R_f = 0.50$ (CH_2Cl_2/AcOEt/*n*-Hex, 1/1/1). ^{1}H NMR (300 MHz, $CDCl_3$): δ 4.25 (s, 5H), 4.26 (s, 5H), 4.38 (st, 2H), 4.59−4.62 (m, 4H), 4.77 (st, 2H), 4.90 (st, 2H), 6.72 (bt, 1H). Anal. Calcd for $C_{23}H_{21}Fe_2NO_2$: C, 60.70; H, 4.65; N, 3.08. Found: C, 60.48; H, 4.78; N, 3.23.

***N*,*N*′-Bis(ferrocenecarbonylmethyl)oxalamide (6).** Yield 47%; mp 198−201 °C; $R_f = 0.63$ (AcOEt/*n*-Hex, 4/1). ^{1}H NMR (300 MHz, $CDCl_3$): δ 4.18 (s, 5H), 4.46−4.53 (m, 4H), 4.79 (bs, 2H), 8.1 (bt, 1H). Anal. Calcd for $C_{26}H_{24}Fe_2N_2O_4$: C, 57.81; H, 4.48; N, 5.19. Found: C, 57.56; H, 4.20; N, 5.41.

(10) Gaussian 03, Revision B.03, Frisch, M. J. et al. Gaussian, Inc., Pittsburgh PA, 2003. For more related references see Supporting Information.
(11) Bartolottiand, L. J.; Fluchick, K. In *Reviews in Computational Chemistry*; Lipkowitz, K. B.; Boyd, B. D., Eds.; VCH: New York, 1996; Vol. 7, pp 187−216.
(12) Becke, A. D. *J. Chem. Phys.* **1993**, *98*, 5648−5652.
(13) Lee, C.; Yang, W.; Parr, R. G. *Phys. Rev. B* **1988**, *37*, 785−789.
(14) The Stuttgart relativistic small core basis sets were obtained from the Extensible Computational Chemistry Environment Basis Set Database, Version 10/29/02, as developed and distributed by the Molecular Science Computing Facility, Environmental and Molecular Sciences Laboratory, which is part of the Pacific Northwest Laboratory, P.O. Box 999, Richland, Washington 99352, and funded by the U.S. Department of Energy. The Pacific Northwest Laboratory is a multiprogram laboratory operated by Battelle Memorial Institute for the U.S. Department of Energy under contract DE-AC06-76RLO 1830.
(15) (a) Barone, V.; Cossi, M. *J. Phys. Chem. A* **1998**, *102*, 1995−2001. (b) Cossi, M.; Rega, N.; Scalmani, G.; Barone, V. *J. Comput. Chem.* **2003**, *24*, 669−681.
(16) Tárraga, A.; Molina, P.; Curiel, D.; Velasco, M. D. *Tetrahedron Lett.* **2002**, *43*, 8453−8457.

***N*-(Phenacyl)ferrocenecarboxamide (8).** Yield 76%; mp 140−143 °C; R_f = 0.39 (CH_2Cl_2/AcOEt/*n*-Hex, 1/1/1). ^{1}H NMR (300 MHz, $CDCl_3$): δ 4.25 (s, 5H), 4.39 (s, 2H), 4.78 (s, 2H), 4.90 (d, 2H, *J*(H,H) = 4.3 Hz), 6.80 (bs, 1H), 7.48−7.65 (m, 3H), 8.04 ppm (d, 2H, *J*(H,H) = 7.2 Hz). Anal. Calcd for $C_{19}H_{17}FeNO_2$: C, 65.73; H, 4.94; N, 4.03. Found: C, 65.63; H, 4.88; N, 4.12.

***N,N′*-Bis(phenacyl)-1,1′-ferrocenedicarboxamide (10).** Yield 53%; mp 179−180 °C; R_f = 0.46 (AcOEt CH_2Cl_2, 7/3). ^{1}H NMR (300 MHz, CDCl): δ 4.49 (s, 4H), 4.88 (d, 2H, *J*(H,H) = 5.9 Hz), 4.92 (s, 4H), 7.48−7.65 (m, 2H), 8.00 (d, 4H, *J*(H,H) = 7.3 Hz), 8.27 (t, 2H, *J*(H,H) = 5.9 Hz). Anal. Calcd for $C_{28}H_{24}FeN_2O_4$: C, 66.16; H, 4.76; N, 5.51. Found: C, 66.38; H, 4.60; N, 5.48.

1,1′-Bis(benzoylaminoacetyl)ferrocene (13). Yield 79%; mp 222−225 °C; R_f = 0.37 (CH_2Cl_2/AcOEt/*n*-Hex, 1/1/1). ^{1}H NMR (300 MHz, $CDCl_3$): δ 4.60 (d, 4H, *J*(H,H) = 4.8 Hz), 4.65 (st, 4H), 4.98 (st, 4H), 7.24 (bt, 2H), 7.39−7.54 (m, 6H), 7.88 (d, 4H, *J*(H,H) = 7.2 Hz). Anal. Calcd for $C_{28}H_{24}FeN_2O_4$: C, 66.16; H, 4.76; N, 5.51. Found: C, 65.93; H, 4.52; N, 5.39.

General Procedure for the Preparation of 2,5-Disubstituted Thiazole Derivatives. To a suspension of the appropriate mono- (0.8 mmol) or bis-β-ketoamide (0.6 mmol) in dry THF (15 mL), Lawesson's reagent (1.6 mmol, for mono- or 2.4 mmol, for bis-β-ketoamides, respectively), was added in one portion. The suspension was heated at reflux under nitrogen for 5 h, and then the solvent was removed under reduced pressure to give the corresponding thiazole derivatives, as crude products, which were column chromatographed on silica gel, using EtOAc/*n*-hexane (7/3) as eluent, and afterward crystallized from CH_2Cl_2/ Et_2O (1/3).

5-Ferrocenyl-2-phenylthiazole (3).[16] Yield 31%; mp 91−94 °C; R_f = 0.85 (CH_2Cl_2/AcOEt/*n*-Hex, 1/1/1). ^{1}H NMR (300 MHz, $CDCl_3$): δ 4.13 (s, 5H), 4.34 (st, 2H), 4.60 (st, 2H), 7.41−7.47 (m, 3H), 7.71 (s, 1H), 7.91−7.97 (m, 2H). Anal. Calcd for $C_{19}H_{15}FeNS$: C, 66.10; H, 4.38; N, 4.06. Found: C, 65.96; H, 4.50; N 4.24.

2,5-Bis(ferrocenyl)thiazole (5).[16] Yield 62%; mp 221−222 °C;[16] R_f = 0.72 (CH_2Cl_2/AcOEt/*n*-Hex, 1/1/1).

5,5′-Bis(ferrocenyl)-2,2′-bis(thiazole) (7). Yield 30%; mp 112−114 °C; R_f = 0.74 (CH_2Cl_2/AcOEt/*n*-Hex, 1/1/1). ^{1}H NMR (300 MHz): δ 4.14 (s, 10H), 4.39 (st, 4H), 4.64 (st, 4H), 7.72 (s, 2H). Anal. Calcd for $C_{26}H_{20}Fe_2N_2S_2$: C, 58.23; H, 3.76; N, 5.22. Found: C, 58.06; H, 3.89; N, 5.04.

2-Ferrocenyl-5-phenylthiazole (9).[16] Yield 74%; mp 156−158 °C; R_f = 0.67 (CH_2Cl_2/AcOEt/*n*-Hex, 1/1/1). ^{1}H NMR (300 MHz, $CDCl_3$): δ 4.15 (s, 5H), 4.43 (st, 2H), 4.89 (st, 2H), 7.25−7.44 (m, 3H), 7.57(m, 2H), 7.83 (s, 1H). Anal. Calcd for $C_{19}H_{15}FeNS$: C, 66.10; H, 4.38; N, 4.06. Found: C, 66.32; H, 4.51; N 3.91.

1,1′-Bis[(5-phenyl)-1,3-thiazol-2-yl]ferrocene (11). Yield 71%; mp 205−206 °C; R_f = 0.41 (AcOEt CH_2Cl_2, 7/3). ^{1}H NMR (300 MHz, $CDCl_3$): δ 4.42 (st, 4H), 4.92 (st, 4H), 7.23−7.27 (m, 6H), 7.32−7.37 (m, 4H), 7.65 (s, 2H). Anal. Calcd for $C_{28}H_{20}FeN_2S_2$: C, 66.67; H, 4.00; N, 5.55. Found: C, 66.90; H, 4.13; N 5.77.

1,1′-Bis[(2-phenyl)-1,3-thiazol-5-yl]ferrocene (14). Yield 43%; mp 165−167 °C; R_f = 0.58 (AcOEt CH_2Cl_2, 7/3). ^{1}H NMR (300 MHz, $CDCl_3$): δ 4.32 (st, 4H), 4.53 (st, 4H), 7.25−7.32 (m, 6H), 7.64−7.76 (m, 6H). Anal. Calcd for $C_{28}H_{20}FeN_2S_2$: C, 66.67; H, 4.00; N, 5.55. Found: C, 66.48; H, 4.19; N 5.38.

Preparation of 1,1′-Bis(α-aminoacetyl)ferrocene Dihydrochloride (12). To a suspension of Pd/C (10%) (0.2 g) in glacial acetic acid (25 mL) was added dropwise a solution of 1,1′-bis(α-azidoacetyl)ferrocene (0.6 g, 1.70 mmol) in CH_2Cl_2 (5 mL), and the reaction mixture was stirred at room temperature for 3 h, while a stream of H_2 was bubbled through the solution. Then, the solution was filtered over a Celite pad which was washed with acetic acid (3 × 15 mL). To the combined filtrates a stream of dry HCl was bubbled for 2 h, and then, the solvent was evaporated under reduced pressure. The resulting oil was triturated with diethyl ether (20 mL) to afford the title compound, in 90% yield, which was used without further purification. IR (Nujol; cm^{-1}): 3405, 2925, 2864, 2614, 1694, 1675, 1588, 1516, 1270, 1079, 880. ^{1}H NMR (300 MHz, $CDCl_3$): δ 4.17 (bs, 4H), 4.84 (bs, 4H), 5.08 (bs, 4H), 8.45 (bs, 4H). ^{13}C NMR (300 MHz, $CDCl_3$): δ 47.8 (2 × CH_2), 73.9 (4 × CH, Cp), 78.5 (4 × CH, Cp), 200.5 (2 × C═O). EIMS (70 eV) *m*/*z* (relative intensity): 300 (100) [M^+ − 2HCl], 271 (98), 254 (44), 178 (54), 165 (70), 121 (70).

Results and Discussion

Synthesis. The general synthetic route for the 2,5-disubstituted thiazole derivatives is based on a two-step sequence. First, acylation of the suitable α-aminocarbonyl compound with the proper acyl chloride in the presence of Et_3N provides the corresponding β-ketoamide intermediate which, in a second step, undergoes a heterocyclization reaction, promoted by the action of the Lawesson's reagent [4-$MeOC_6H_4P(S)S]_2$ (LR), to afford the suitable disubstituted thiazole ring. In this approach, the substituent at position 5 of the thiazole ring arises from the α-aminocarbonyl compound, whereas the substituent at position 2 comes from the acyl chloride component. Using this methodology, compounds **3**, **5**, and **7** were prepared in 31%, 62%, and 30% yields, respectively, starting from of α-aminoacetylferrocene[7e] **1** and using benzoyl chloride, chlorocarbonyl ferrocene, or oxalyl choride, respectively, as acylating agents (Scheme 1).

Likewise, starting from phenacylamine and using chlorocarbonyl ferrocene or 1,1′-dichlorocarbonyl ferrocene as acylating reagents, the monoferrocenyl-thiazole **9** and 1,1′-bisthiazolyl ferrocene, **11**, were obtained in 74% and 71% yields, respectively (Scheme 2).

On the other hand, 1,1′-bis(2-phenylthiazol-5-yl)ferrocene **14** was also obtained, in 43% yield, from the reaction of benzoyl chloride with the previously unreported 1,1′-bis(α-aminoacetyl)ferrocene **12**, synthesized by catalytic hydrogenation of 1,1′-bis(α-azidoacetyl)ferrocene[7d] (Scheme 3). Spectral (MS and ^{1}H and ^{13}C NMR) and elemental analysis data of both the newly synthesized β-ketoamide intermediates and thiazole derivatives are consistent with the proposed structures.

Molecular Structures. Single crystals of compounds **3**, **5**, **11**, and **14**, suitable for X-ray structure determination, were grown from diffusion of *n*-hexane into a solution of the compound in CH_2Cl_2 or by slow evaporation of the solvent. Unfortunately, all attempts to grow good quality single crystals of compounds **7** and **9** failed.

Compound **3** crystallizes in the monoclinic space group $P2_1/n$ with four molecules in the unit cell. Figure 1a shows the ORTEP drawing of the molecular structure of **3** with the atomic numbering scheme. The two Cp rings have a small tilt angle between them, and the angle between the mean planes of the bridged Cp and the attached thiazole ring is 2.5°. Moreover, the angle between the thiazole plane and the attached phenyl ring, linked at the 2 position of the

Scheme 1. Synthesis of Compounds **3**, **5**, and **7**

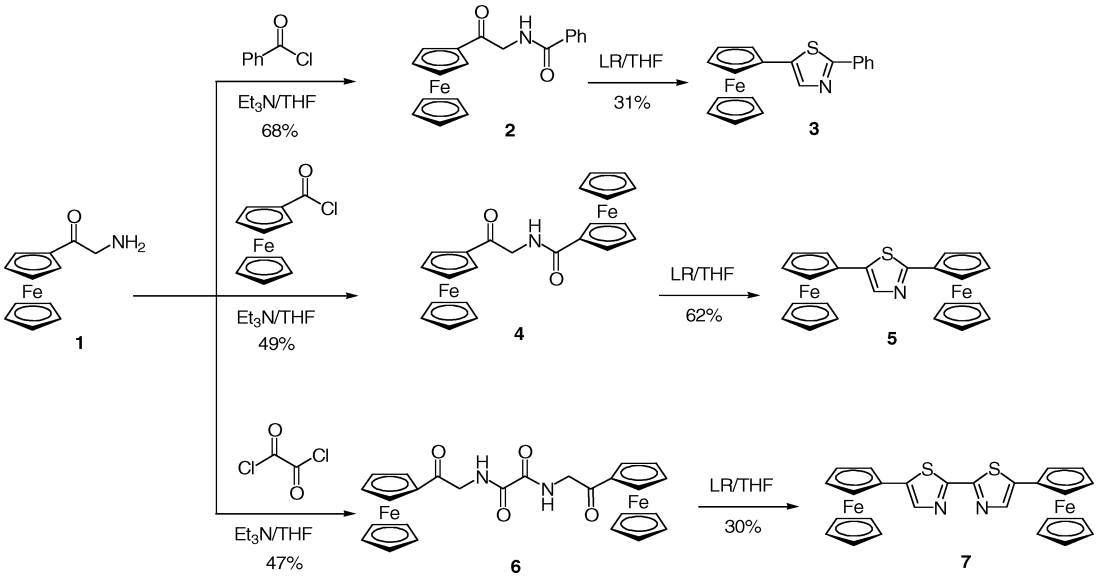

Scheme 2. Synthesis of Compounds **9** and **11**

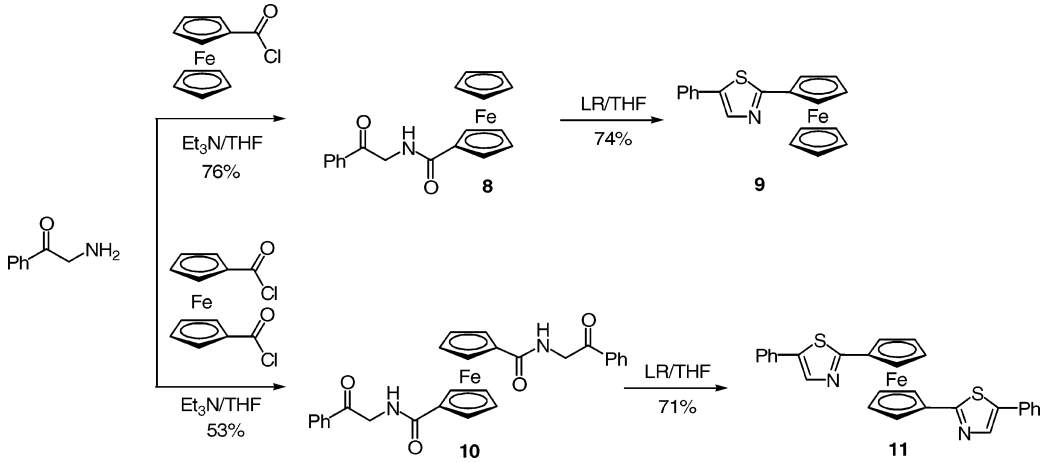

Scheme 3. Synthesis of Compound **14**

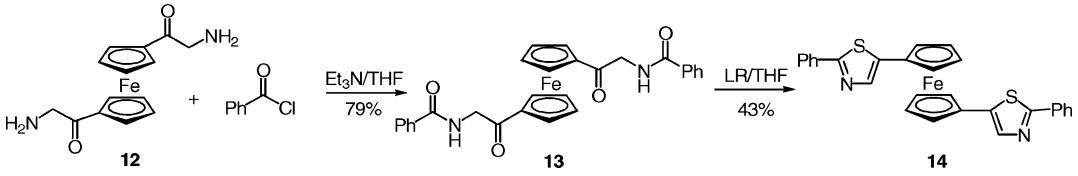

bridge, is 3.4°. Thus, all the atoms of the thiazole bridge and the two attached rings are disposed in a planar conformation indicating a large degree of π conjugation in this compound. Molecules of **3** pack in the crystal (see Figure S1 in Supporting Information) in groups of two molecules in a head-to-tail arrangement, and these groups are stacked along the *b*-axis in a herringbone fashion.

Compound **5** crystallizes in the orthorhombic space group *Pccn* with eight molecules in the unit cell. Figure 1b shows the ORTEP drawing of the molecular structure of **5** with the atomic numbering scheme. The molecular structure reveals a 1:1 occupation disorder of the N1(═C2A):C2(═N1A) unit which is probably originated by the absence of significant directional intermolecular interactions that fix the relative position of N atoms, a situation that arises from the predominant role played by the ferrocene groups in the crystal packing. Cp rings in each independent ferrocene unit have very small tilt angles between them. The two Cp rings of ferrocene **2** are essentially eclipsed while those in ferrocene **1** are less eclipsed. The angles between the mean planes of the bridged Cp ring of ferrocenes **1** and **2** and the attached thiazole ring are 3.2° and 2.6°, respectively. Thus, all the atoms of the thiazole bridge and the two attached rings are disposed in an almost completely planar conformation indicating also a large degree of π conjugation in this compound. Molecules of **5** pack in the crystal (see Figure S2 in Supporting Information) in groups of four molecules adopting a rhombic clusters when viewed along the *c*-axes and such rhombic molecular clusters are packed parallel along the *ab*-plane.

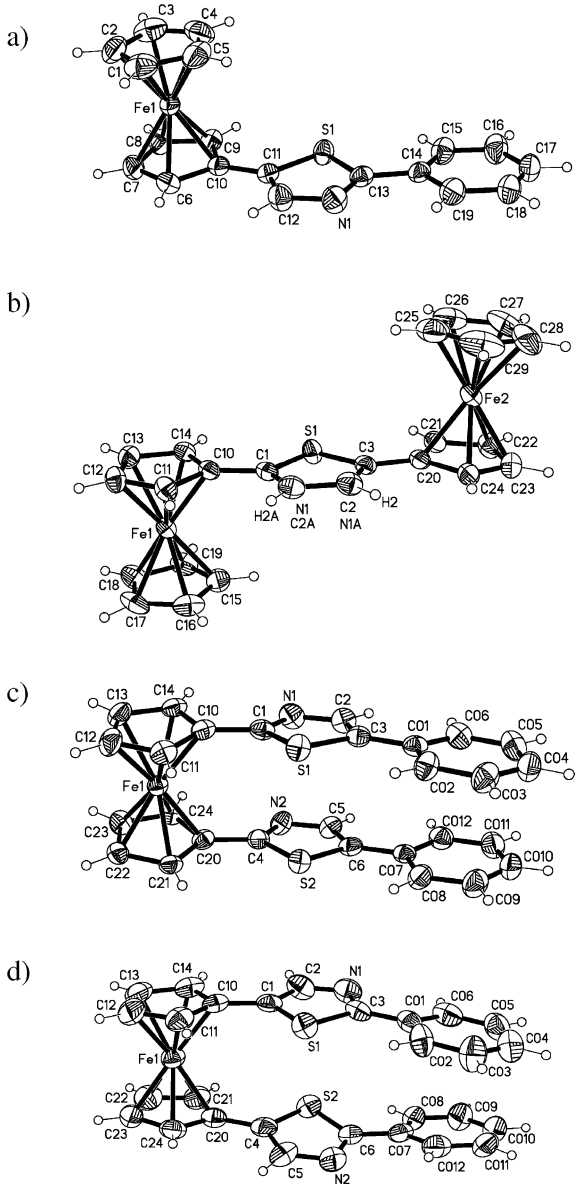

Figure 1. ORTEP view of the molecular structure of compounds **3** (a), **5** (b), **11** (c), and **14** (d) showing the atom labeling in the asymmetric unit. Thermal ellipsoids are drawn at 50% probability level.

Compounds **11** and **14** are well ordered, but both are racemic twins with an accidentally similar twin ratio of 0.52:0.48. Compound **11** crystallizes in the monoclinic space group $P2_1$ with two molecules in the unit cell while compound **14** crystallizes in the orthorhombic space group $P2_12_12_1$. Figure 1c,d shows the ORTEP drawings of the molecular structures of **11** and **14** with the corresponding atomic numbering schemes. The two Cp rings in the two compounds have small tilt angles between them and are nearly eclipsed in **11** and less eclipsed in **14**. The angles between the mean planes of the Cp rings and the attached thiazole rings are 11.8° and 11.5° in **11** and 2.8° and 10.9° in **14**. Moreover, the angles between the thiazole planes and the attached phenyl rings are 3.0° and 3.4° in **11** and 7.5° and 16.2° in **14**. Thus, while in compound **11** the planes of the two thiazole bridges and the attached phenyl rings are almost parallel to each other, those in compound **14** are somewhat less coplanar.

Table 1. UV−Vis Absorption and Electrochemical Data of the Studied Compounds

compd	$\lambda_{max}{}^a$ (10^{-3} ϵ)	$E_{1/2}{}^b$ [L]	$E_{1/2}{}^{b,c}$ [LH^{n+}]
3	327 (14.9), 449 (1.2)	0.52	0.59
5	327 (11.6), 457 (1.7)	0.49, 0.63	0.63
7	369 (10.6), 486 (3.8)	0.55	
9	326 (13.7), 459 (0.99)	0.57	0.72
11	320 (29.8), 469 (1.6)	0.67	
14	321 (23.5), 459 (1.6)	0.58	

[a] λ_{max}, in nm; ϵ, in dm^3 mol^{-1} cm^{-1}. Spectra were made in CH_2Cl_2 solutions ($c = 1 \times 10^{-4}$M). [b] Volts vs SCE, Pt working electrode, CH_2Cl_2 containing 1 M $[(n\text{-Bu})_4N]ClO_4$, 20 °C. [c] $n = 1$ for **3**, **5**, and **9**; $n = 2$ for **7**, **11**, and **14**.

Molecules of **11** pack in the crystal (see Figure S3 in Supporting Information) in a herringbone arrangement along the *b*-axes forming chains which are disposed perpendicularly to each other along the *c*-axes. Molecules of **14** pack in the crystal (see Figure S4 in Supporting Information) forming layers in the *ac*-plane in which the molecules adopt a herringbone distribution along the *a*-axes. Molecules belonging to neighboring layers are inverted 180°.

Atomic distances and bond angles of all four compounds are close to those previously observed for ferrocene[17] and other substituted ferrocene compounds.[6c,8a,c]

Redox and Optical Properties. Reversibility and relative potentials of redox processes in the compounds were determined by cyclic (CV) and differential pulse (DPV) voltammetry[18] in 10^{-3} M acetonitrile/dichloromethane (3/2) solutions containing 0.1 M $[(n\text{-Bu})_4N]ClO_4$. Oxidation potentials of compounds **3**, **9**, **11**, and **14** were used to determine the influence of the substitution pattern between the ferrocene and thiazole groups in the electronic interaction between the two units in the isomeric derivatives (Table 1). Likewise, CV and DPV were also used to evaluate the strength of the interaction between the metal centers in the homobimetallic complexes **5** and **7** (Table 1).

The cyclic voltammograms of the monoferrocenyl derivatives **3** and **9**, which display a single anodic process with features of chemical and electrochemical reversibility, showed that 5-ferrocenylthiazole **3** is more easily oxidized by 50 mV than the isomeric 2-ferrocenylthiazole **9**. This is in agreement with the predictions from the MO calculations of varying degrees of sophistication of the thiazole ring, which predict a slightly higher electron density at position C(5) than C(2).[19]

The CV data of the isomeric 1,1′-bis(thiazolyl)ferrocenes **11** and **14**, which display a reversible redox wave, showed that compound **14**, bearing 5-substituted thiazole rings, is more easily oxidized by 90 mV than **11**, with 2-substituted thiazole rings, indicating not only that the introduction of a

(17) Séller, P.; Dunitz, J. D. *Acta Crystallogr., Sect. B* **1982**, *38*, 1741−1745.
(18) All processes observed were reversible, according to the criteria of (i) separation of 60 mV between cathodic and anodic peaks, (ii) close-to-unity ratio of the intensities of the cathodic and anodic currents, and (iii) constancy of the peak potential on changing sweep rate in the CVs. The same halfwave potential values have been obtained from the DPV peaks and from an average of the cathodic and anodic cyclic voltammetric peak.
(19) Metzger J. V. In *Comprehensive Heterocyclic Chemistry*; Katritzky, A. R., Rees, C. W., Eds.; Pergamon: Oxford, U.K., 1984; Vol. 6, Chapter 4.19, pp 226−331.

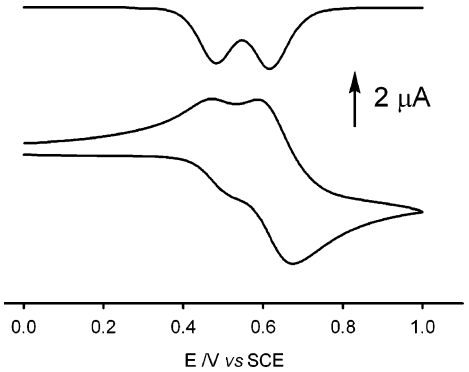

Figure 2. DPV (upper) and CV (lower) of compound **5** (1 mM), in CH_2Cl_2/CH_3CN (3/2) using $[(n\text{-}Bu)_4N]ClO_4$ as supporting electrolyte and scanned at 100 mV s^{-1} from 0 to 1 V.

second thiazole ring in the unsubstituted cyclopentadienyl ring of **3** and **9** gives rise to addition effects but also that there is electrochemical evidence of the stronger electron-withdrawing character of the 2 position of the thiazole ring than the 5 position.

The CV of **5** (Figure 2) shows two closely spaced reversible one-electron oxidations for the ferrocenyl groups. Likewise, the DPV voltammogram (Figure 2) also exhibits two well resolved oxidation waves of the same area. It is worth noting that in compound **5** the ferrocene subunit at 5 position is more easily oxidized by 30 mV than the ferrocene group in model compound **3**, whereas the ferrocene subunit at 2 position is more difficult to oxidize by 60 mV than in model compound **9**. These results could be explained by the fact that the phenyl group is a weaker electron-donating group than ferrocenyl unit and the ferrocenium group is a stronger electron-withdrawing group than phenyl ring.

The comproportionation constant K_c for $\mathbf{5}^{\bullet+}$ was calculated,[20] from the observed wave splitting, $\Delta E_{1/2} = 140$ mV, resulting in a value of $K_c = 2.32 \times 10^2$ from which a free energy of comproportionation, $\Delta G_c°$, of 1128 cm^{-1} is obtained. The $\Delta E_{1/2}$ (and $\Delta G_c°$) value may be used for the assessment of the extent of ferrocenyl−ferrocenyl coupling although it only provides an approximate value of such an interaction because this magnitude has been shown to be extremely medium-dependent[21] and contains additional contributions that are difficult to estimate for delocalized systems, such as the statistical contribution ($^1/_2RT$ ln $^1/_4$), the electrostatic interaction arising from the repulsion of two similarly charged metal centers, and the synergistic factor due to metal−ligand backbonding interaction. Nevertheless, comparison of the $\Delta E_{1/2}$ (and $\Delta G_c°$) value of **5** with those shown by other similar bisferrocenyl compounds provides a qualitative estimation of the actual metal−metal electronic coupling. Thus, the wave splitting in compound **5** ($\Delta E_{1/2} =$ 140 mV) is smaller than those for 1,4-bis(ferrocenyl)-2-aza-1,3-butadiene[8a] ($\Delta E_{1/2} = 210$ mV), whereas the value is slightly larger than those observed for most bis-ferrocenyl compounds with carbon-chain π-conjugated bridges, such as 1,4-bis(ferrocenyl)-1,3-butadiene[22] ($\Delta E_{1/2} = 129$ mV) and 1,4-bis(ferrocenyl)butadiyne[23] ($\Delta E_{1/2} = 120$ mV) indicating the presence of a certain strength in the metal−metal coupling.

Finally, the voltammograms of compound **7**, containing two ferrocenyl groups linked through a 2,2′-bis(thiazole) unit, show only a reversible two-electron oxidation wave, indicating that there is little or a null direct interaction between the metal centers over the large conjugated bis-heterocyclic bridge.

The UV−vis data obtained in CH_2Cl_2 for the mono- and bis-thiazolyl ferrocenes are collected in Table 1; they are consistent with most ferrocenyl chromophores in that they exhibit two charge-transfer bands in the visible region.[24] These spectra contain a prominent absorption band with a maximum between 320 nm, for **11**, and 369 nm, for **7**, which can safely be ascribed to ligand-centered $\pi-\pi^*$ electronic transitions ($L-\pi^*$) (HE band) (Table 1). In addition to this band, another weaker absorption is detected between 449 nm, for **3**, and 486 nm, for **7**, which is assigned to another localized excitation with a lower energy produced either by two nearly degenerate transitions: a Fe(II) d−d transition[25] or by a metal−ligand charge transfer (MLCT) process ($d_\pi-\pi^*$) (LE band). This assignment is in accordance with the latest theoretical treatment (model III) reported by Barlow et al.[26]

Spectroelectrochemical Studies. The generation of the oxidized species derived from **3**, **9**, **11**, and **14** was performed electrochemically and monitored by absorption spectroscopy. Stepwise Coulommetric titrations were performed on ca. 3.5 $\times 10^{-3}$ mol·L^{-1} solutions of these complexes in CH_2Cl_2, with $[(n\text{-}Bu)_4N]PF_6$ (0.15 M) as supporting electrolyte, and the absorption spectra were regularly recorded for different average number ($0 \le n \le 1$) of removed electrons. UV−vis−near-IR spectral data of $\mathbf{3}^{\bullet+}$, $\mathbf{9}^{\bullet+}$, $\mathbf{11}^{\bullet+}$, and $\mathbf{14}^{\bullet+}$ are collected in Table 2.

Spectra of $\mathbf{3}^{\bullet+}$, $\mathbf{9}^{\bullet+}$, $\mathbf{11}^{\bullet+}$, and $\mathbf{14}^{\bullet+}$ show three main groups of absorption bands. The high-energy absorptions in the UV appear at similar wavelengths and show comparable intensities to the HE bands exhibited by the corresponding neutral complexes **3**, **9**, **11**, and **14**. The absorption bands in the NIR region, which are not observed in the neutral complexes, are assigned to a thiazole → Fe^{III} LMCT transition. This assignment is based on the following considerations: (i) during the course of the oxidations of complexes **3**, **9**, **11**, and **14**, these low-energy bands increase continuously in intensity, achieving their maximum when the oxidation

(20) Richarson, D. E.; Taube, H. *Inorg. Chem.* **1981**, *20*, 1278−1285.
(21) Barriere, F.; Camire, N.; Geiger, W. E.; Mueller-Westerhoff, U. T.; Sanders, R. *J. Am. Chem. Soc.* **2002**, *124*, 7262−7263.
(22) Ribou, A. C.; Launay, J. P.; Sachtleben, M. L.; Li, M.; Spangler, C. W. *Inorg. Chem.* **1996**, *35*, 3735−3740.
(23) LeVanda, C.; Bechgaard, K.; Cowan, D. O. *J. Org. Chem.* **1976**, *41*, 2700−2704.
(24) Farrel, T.; Meyer-Friedrichsen, T.; Malessa, M.; Haase, D.; Saak, W.; Asselberghs, I.; Wostyn, K.; Clays, K.; Persoons, A.; Heck, J.; Manning, A. R. *J. Chem. Soc., Dalton Trans.* **2001**, 29−36 and references therein.
(25) (a) Geoffroy, G. L.; Wrighton, M. S. *Organometallic Photochemistry*; Academic Press: New York, 1979. (b) Sohn, Y. S.; Hendrickson, D. N.; Gray, H. B. *J. Am. Chem. Soc.* **1971**, *93*, 3603−3612.
(26) Barlow, S.; Bunting, H. E.; Ringham, C.; Green, J. C.; Bublitz, G. U.; Boxer, S. G.; Perry, J. W.; Marder, S. R. *J. Am. Chem. Soc.* **1999**, *121*, 3715−3723.

Table 2. UV−Vis−Near-IR Absorption Data of the Oxidized Compounds

compd	λ_{max} (10^{-3} ϵ)[a]	
$\mathbf{3}^{+}$	323(>14.0),415(5.2),478(2.4), 591(0.28)	818 (0.46), 932 (0.43)
$\mathbf{5}^{+}$	316(10.8),352(8.0),409(4.6), 535(2.5)	810 (0.25), 1355 (0.32)
$\mathbf{5}^{2+}$	350(8.1),398(sh),470(sh), 556(0.99)	791 (0.75)
$\mathbf{7}^{2+}$	376(17.5), 435 (sh),564(sh)	834 (0.95)
$\mathbf{9}^{+}$	349(> 8.0), 481(2.5), 570(sh)	816 (0.39), 927 (0.28)
$\mathbf{11}^{+}$	334(> 13.0),405(6.9), 495(3.1)	855 (0.49), 1018 (0.58)
$\mathbf{14}^{+}$	319(26.6), 387(8.2), 487(2.8)	867 (0.62), 1019 (0.77)

[a] λ_{max}, in nm; ϵ, in dm^3 mol^{-1} cm^{-1}. Spectra were made in CH_2Cl_2 with [(*n*-Bu)$_4$N]PF_6 (0.15 M).

process is completed (see Figure S12 in Supporting Information). (ii) Similar low-energy transitions have been observed in the NIR region in other Fe^{III} and Ru^{III} complexes with conjugated oligothiophene ligands,[27,28] having $-CH_2-N(R)-CH_2-$ and $-CH-N-CH-CH-$ (2-aza-1,3-butadiene) as bridges.[8a,29] (iii) A thiazole ring can structurally be viewed as a 2-aza-1,3-butadiene closed by a sulfur atom having hereby a similar electronic structure. Therefore, the absorption bands in the NIR exhibited by $\mathbf{3}^{\bullet+}$, $\mathbf{9}^{\bullet+}$, $\mathbf{11}^{\bullet+}$, and $\mathbf{14}^{\bullet+}$ are assigned to an optically induced electron transfer from the thiazole to the Fe^{III} center.

Oxidized species derived from **5** were also generated and studied in the same way as the other four compounds, and absorption spectra were regularly recorded for different numbers ($0 \le n \le 2$) of removed electrons. Figure 3 exhibits the evolution of the spectra during the oxidation of **5** in the $0 \le n \le 1$ range showing an increase of the Cp → Fe^{III} LMCT bands appearing at 409 and 535 nm, which is characteristic of a ferrocenium ion. Besides, a decrease of the band at 457 nm is observed, which corresponds to a localized excitation of a ferrocene group. Along with the changes of these bands, the appearance and maintenance of three well-defined isosbestic points at 234, 321, and 347 nm were observed. Nevertheless, the most interesting feature detected is that during the oxidation of **5** two new bands appeared: one which is weak and centered at 810 nm, and another one, at 1355 nm, which is broad. Their intensities continuously grow until one electron is removed, i.e., when the formation of $\mathbf{5}^{\bullet+}$ is completed. On removing more electrons ($1 \le n \le 2$), the intensity of the first band continues increasing while the band at 1355 nm decreases until it disappears when the dication $\mathbf{5}^{2+}$ is completely formed. Table 2 collects all the spectral data for oxidized complexes $\mathbf{5}^{\bullet+}$ and $\mathbf{5}^{2+}$.

The deconvolution of the experimental spectrum of $\mathbf{5}^{\bullet+}$ in the NIR region, assuming Gaussian shapes in the wavenumber domain (Figure 3), allows an accurate determination

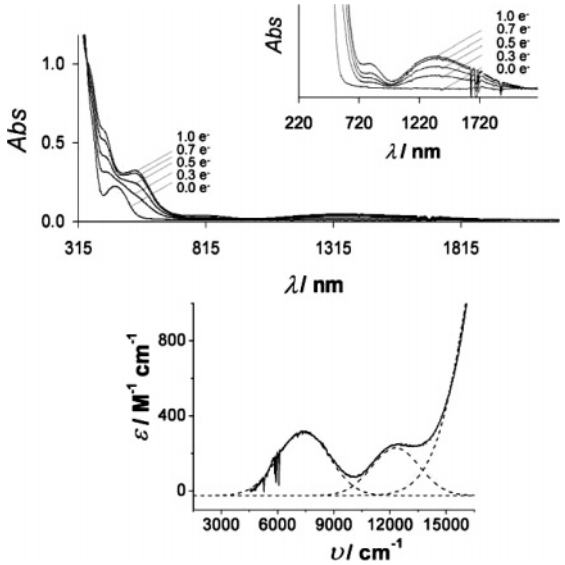

Figure 3. Top: Evolution of vis−near-IR spectra during the course of the oxidation of compound **5**. Inset: near-IR region enlargement. The average number of removed electrons is given on each spectrum. Bottom: Deconvolution of NIR spectrum of $\mathbf{5}^{\bullet+}PF_6^-$ salt. The experimental spectrum was deconvoluted by means of three Gaussian functions (---). The sum of the dashed lines (___) closely matches the experimental spectrum (−).

of the position, width, and intensity of the two observed CT bands, which are gathered in Table 3.[30] These spectral parameters are relevant for the characterization of intramolecular electron-transfer phenomena occurring in $\mathbf{5}^{\bullet+}$.[31]

The presence of several NIR bands in the spectrum of a mixed-valence complex is not uncommon, and their occurrence is generally explained by means of three different possible causes.[32,33] The first one could be the presence of a strong spin−orbit coupling effect, which becomes important only for complexes composed by third-row transition metals.[32] A second origin for these bands could be the presence of a double-exchange mechanism,[33] a mechanism that becomes more likely as the bridge length and the level of π-orbitals increase. Finally, such multiple NIR bands might be caused by the presence of a bridge with accessible electronic state levels or with redox active bridges, as has been recently proposed to explain the rich absorption spectra of certain mixed-valence compounds with redox active bridges.[34] On the basis of the behavior of $\mathbf{3}^{\bullet+}$, $\mathbf{9}^{\bullet+}$, $\mathbf{11}^{\bullet+}$, and

(27) (a) Zu, Y. B.; Wolff, M. O. *Chem. Mater.* **1999**, *11*, 2995−3001. (b) Zu, Y. B.; Millet, D. B.; Wolf, M. O.; Rettig, S. J. *Organometallics* **1999**, *18*, 1930−1938.
(28) Zu, Y. B.; Wolf, M. O. *J. Am. Chem. Soc.* **2000**, *122*, 10121−10125.
(29) (a) Yamaguchi, I.; Sakano, T.; Ishii, H.; Osakada, K.; Yamamoto, T. *J. Organomet. Chem.* **1999**, *584*, 213−216. (b) Horie, M.; Sakano, T.; Osakada, K.; Nakao, H. *Organometallics* **2004**, *23*, 18−20. (c) Horie, M.; Suzaki, Y.; Osakada, K. *J. Am. Chem. Soc.* **2004**, *126*, 3684−3685.
(30) Gould, I. R.; Noukakis, D.; Gómez-Jahn, L.; Young, R. H.; Goodman, J. L.; Farid, S. *Chem. Phys.* **1993**, *176*, 439−456.
(31) The proportion of mixed valence species at half-oxidation (*P*), where $P = K_c^{1/2}/(2 + K_c^{1/2})$, is generally used to compute the intensity of corrected spectra. The comproportionation constant K_c, which is related to the thermodynamic stability of the mixed-valence compound, of the equilibrium of comproportionation, $[Fe^{II}-L-Fe^{II}] + [Fe^{III}-L-Fe^{III}] \leftrightarrows 2[Fe^{II}-L-Fe^{III}]$, was calculated for 5 from the electrochemical data, resulting a value of $K_c = 226$ which yields values of *P* about 90 % and $\epsilon_{corr} = 315$ M^{-1} cm^{-1}.
(32) (a) Kober, E. M.; Goldsby, K. A.; Narayane, D. N. S.; Meyer, T. J. *J. Am. Chem. Soc.* **1983**, *105*, 4303−4309. (b) Lay, P. A.; Magnuson, R. H.; Taube, H. *Inorg. Chem.* **1988**, *27*, 2364−2371. (c) Laidlaw, W. M.; Denning, R. G. *J. Chem. Soc., Dalton Trans.* **1994**, 1987−1994.
(33) (a) Richardson, D. E.; Taube, H. *J. Am. Chem. Soc.* **1983**, *105*, 40−51. (b) Halpern, J.; Orgel, L. E. *Discuss. Faraday Soc.* **1960**, *29*, 32−41.
(34) Nelsen, S. F.; Ismagilov, R. F.; Powell, D. F. *J. Am. Chem. Soc.* **1998**, *120*, 1924−1925.

Table 3. IVCT Band Parameters ($h\nu_{max}$, ϵ_{max}, and $\Delta\nu_{1/2}°$) Obtained from the Spectral Deconvolution and Calculated IET Parameters (V_{ab}) for Radical Cation $\mathbf{5}^{+\bullet}$

IVCT band	$h\nu_{max}$/cm^{-1}	ϵ_{max}/M^{-1} cm^{-1}	$\Delta\nu_{1/2}°$/cm^{-1}	f,[a] 10^{+3}	d[b]/Å	V_{ab}/cm^{-1}
LMCT	12346	250	2570	2.96	5.175	354 (V_{LM})
MMCT	7380	315	2700	3.90	8.407	193 (V_{MM})

[a] Total oscillator strength obtained by $f = 4.6 \times 10^{-9}\epsilon_{max}\Delta\nu_{1/2}$. [b] Effective electron-transfer distances between electroactive sites taken as distances between Fe−Fe′ and Fe−N atoms.

$\mathbf{14}^{\bullet+}$, the latter case seems to be the most feasible for the two NIR bands of $\mathbf{5}^{\bullet+}$. Accordingly, also on the basis of the spectral evolution observed during the oxidation of **5**, the band centered at 810 nm is assigned to a thiazole → Fe^{III} LMCT transition. This result probably implies a photoinduced electron transfer from the N atom of the thiazole bridge to the Fe^{III} site linked at the 5 position of the bridge. On the other hand, the band centered at 1355 nm is attributed to the bridge-mediated superexchange between the two coupled iron sites (M and M′) or an IET between the two iron sites; i.e., to an MM′CT transition.

The application of the two-state Hush[1,3a,35] model to the lowest energy MM′CT band observed in the spectrum of the mixed-valence compound $\mathbf{5}^{\bullet+}$ predicts a half-height bandwidth, $\Delta\nu_{1/2}$, of 3800 cm^{-1}; as calculated from $\Delta\nu_{1/2} = (2310\lambda)^{1/2}$, where λ is the total reorganization energy of Marcus theory which was determined from the observed energy of the MM′CT, $h\nu_{max}$, and the free energy of comproportionation in order to take into account the inequivalent redox sites of the system.[36] Such a predicted $\Delta\nu_{1/2}$ value is larger than the value determined experimentally, $\Delta\nu_{1/2}° = 2700$ cm^{-1}, by the spectral deconvolution assuming Gaussian profiles. This result suggests a considerable degree of electronic delocalization in the ground state of $\mathbf{5}^{\bullet+}$. The availability of the energy of the MM′CT transition, $h\nu_{max}$, also enables the estimation of the electronic coupling parameter between the two metal sites, $V_{MM'}$, of 193 cm^{-1} (adiabatic electronic coupling element), which can be used to gauge the degree of the ground-state delocalization, given by the coefficient $\alpha^2 = 0.026$.[37] Since the Hush model can only be rigorously applied to weakly coupled mixed-valence species, the electrochemical, intermetallic charge transfer study, and the overestimation of the bandwidth compared with the theoretical value,[38] suggest that the $\mathbf{5}^{\bullet+}$ system lies between the class II and the class II−III transition classifications for mixed-valence compounds.[39] The parameter Γ, determined from the experimental and predicted MM′CT bandwidths, provides a useful criterion for determining whether a particular system is weakly coupled, moderately coupled, at the class II−III transition, or strongly coupled (class III).[40] Thus, the resulting value of $\Gamma = 0.29$ indicates that $\mathbf{5}^{\bullet+}$ is a moderately coupled class II system.

On the other hand, the calculated value of $V_{MM'}$ is somewhat smaller than that obtained for 1,4-bis(ferrocenyl)-2-aza-1,3-butadiene,[8a] showing that, as expected for a heteroaromatic bridge,[7] the electronic communication in the closed structure (ring) is a little bit worse than in the open chain bridge.

Oxidized species derived from **7** were also generated electrochemically, and their formation followed by absorption spectroscopy, under the same conditions used for compound **5**. However, in this case no intervalence band was observed, which implies no intramolecular electron transfer. Presumably, the length of the bis-heteroaromatic bridge in **5** precludes electron coupling, as also indicated by its CV, which has a single reversible oxidation wave only.

Finally, compounds $\mathbf{3}^{\bullet+}$, $\mathbf{9}^{\bullet+}$, $\mathbf{11}^{\bullet+}$, $\mathbf{14}^{\bullet+}$, $\mathbf{5}^{\bullet+}$, $\mathbf{5}^{2+}$, and $\mathbf{7}^{2+}$ were characterized by EPR presenting the typical pattern signals corresponding to a low-spin Fe^{III} species (see the EPR data in Supporting Information).

Ion Sensing Properties. One of the most interesting attributes of the new ferrocene-thiazole compounds reported here is the presence of at least one metal-ion binding site on the thiazole ring which is in proximity to a ferrocene redox-active moiety. Due to this structural feature, the detailed study of their protonation[41] and metal-recognition properties was of interest. At first, the electrochemical behavior of these new ferrocenyl thiazole ligands in the presence of variable concentrations of HBF_4 was investigated. With addition of stoichiometric quantities of HBF_4 in CH_3CN to a solution of compounds **3** and **9** in CH_3CN/CH_2Cl_2 (3:2), the redox potential of the ferrocene nucleus was shifted anodically. The protonation-induced redox potential shift was higher for compound **9** ($\Delta E_{1/2} = 152$ mV) than for compound **3** ($\Delta E_{1/2} = 72$ mV). These values are in good agreement with the linear relationship between the inverse iron−nitrogen separa-

(35) (a) Creutz, C. *Prog. Inorg. Chem.* **1983**, *30*, 1−73. (b) Nelsen, S. F. *Chem. Eur. J.* **2000**, *6*, 581−588.

(36) Hush theory indicates that, for a mixed-valence systems with two inequivalent redox centers, the energy of the IVCT transition is given by $h\nu_{max} = \lambda + \Delta G_c^*$, where λ is the reorganization energy of Marcus, and theory and ΔG_c^* can be estimated from the electrochemical data. For an elegant application see: Barlow, S. *Inorg. Chem.* **2001**, *40*, 7047−7053.

(37) $V_{ab} = 2.05 \times 10^{-2}$ $(\epsilon_{max}\Delta\nu^{1/2}\nu_{max})^{1/2}/r$ is the Hush equation for the calculation of the electronic interaction in mixed-valence complexes and $\alpha = (V_{ab}/h\nu_{max})$ was used to estimate the degree of electronic delocalization.

(38) The origin of this discrepancy is not immediately clear, although differences between theoretical and experimental values of $\Delta\nu_{1/2}$ are not uncommon. They often arise from system nonidealities with respect to the model. See: (a) Elliot, C. M.; Derr, D. L.; Matyushov, D. V.; Newton, M. D. *J. Am. Chem. Soc.* **1998**, *120*, 11714−11726. (b) Curtis, J. C.; Meyer, T. J. *Inorg. Chem.* **1982**, *21*, 1562−1571.

(39) Demadis, K. D.; Hartshorn, C. M.; Meyer, T. J. *Chem. Rev.* **2001**, *101*, 2655−2685.

(40) The magnitude of the Γ parameter, $\Gamma = 1 - (\Delta\nu_{1/2}/\Delta\nu°_{1/2})$, distinguishes the class of mixed-valence system: $0 < \Gamma < 0.1$ for weakly coupled class II system; $0.1 < \Gamma < 0.5$ for moderately-coupled class II systems; $\Gamma = 0.5$ at the transition between class II and class III; and $\Gamma > 0.5$ for class III. See: (a) Brunschwig, B. S.; Creutz, C.; Sutin, N. *Chem. Soc. Rev.* **2002**, *31*, 168−184. (b) D'Alessandro, D. M.; Keene, F. K. *Chem. Soc. Rev.* **2006**, *35*, 424−440.

(41) Previous studies related to the protonation of compounds **3**, **5**, and **9** have already been published in a short communication. See ref 16.

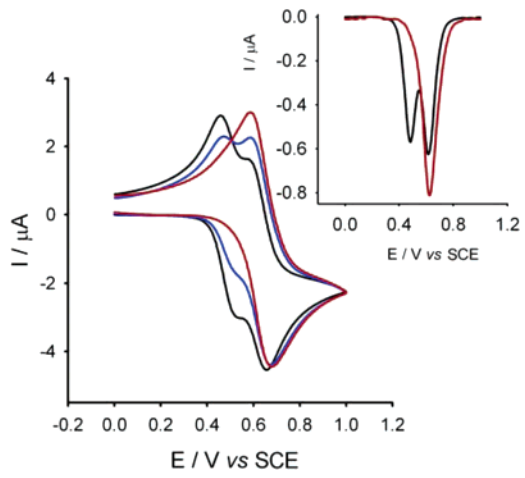

Figure 4. Cyclic voltammogram of compound **5** (1 mM), in CH_2Cl_2/CH_3CN (3/2) using $[(n\text{-}Bu)_4N]ClO_4$ as supporting electrolyte scanned at 100 mV s^{-1} from 0 to 1 V (black), after addition of 0.5 equiv of HBF_4 (blue) and 1 equiv of HBF_4 (red). Inset: DPV of compound **5** (1 mM), in CH_2Cl_2/CH_3CN (3/2) using $[(n\text{-}Bu)_4N]ClO_4$ as supporting electrolyte scanned at 100 mV s^{-1} from 0 to 1 V (black) and after addition of 1 equiv of HBF_4 (red).

tion and the shifts of the potentials found upon protonation for several kinds of aza-substituted ferrocenes.[42]

Unfortunately, it was not possible to investigate the effect of the addition of HBF_4 on the redox chemistry of ligand **11** because H^+ promoted the formation of the corresponding very insoluble thiazolium salt immediately. Nevertheless, for ligand **14**, a new redox wave evolved on addition of 2 equiv of HBF_4, which was shifted 134 mV anodically from the original ferrocene redox potential in the neutral ligand. Compound **14**, however, showed a more complex perturbation of the redox wave on addition of substoichiometric amounts of HBF_4. The original wave was shifted and resolved progressively as the proton addition was increased until 2 equiv of acid was added.

Curiously, the cyclic voltammogram of compound **5**, upon protonation under the same conditions, showed a clear evolution of the first wave from $E_{1/2} = 0.49$ to 0.63 V whereas there was no effect on the second one. Remarkably, the current intensity of the cathodic peak of the second wave increases, while that of the first one decreases with a linear dependence on the equivalents of the added acid. In particular, the second wave reaches the maximum current intensity value at 1.0 equiv of added acid, and at this point the first wave disappears (Figure 4). The occurrence of this wave at the same potential as that for unprotonated **5** suggests that, after oxidation of the ferrocene unit linked at 5-position, the adduct is deprotonated and a subsequent oxidation takes place on the partially oxidized $\mathbf{5}^{\bullet+}$. In other words, these results show that the $\mathbf{5}\cdot H^+$ adduct undergoes reversible electrochemically induced deprotonation/reprotonation processes on a time scale faster than that of the electrochemical experiments, at 100 mV s^{-1}. It is noteworthy that the reversibility of the chemical process is confirmed by the fact that the CV and DPV of the adduct $\mathbf{5}\cdot H^+$, recorded after base addition, is identical to that obtained before the addition of acid.

A similar electrochemical study carried out on receptor **7** reveals that addition of HBF_4 to an electrochemical solution of the ligand in CH_3CN/CH_2Cl_2 (3:2) does not cause any change in the redox potential of the ferrocene moiety.

Having proven the ability of ferrocenylthiazoles to offer an electrochemical response to a variation in the concentration of H^+, the electrochemical behavior of these receptors was also investigated in the presence of several divalent metal ions, such as Ca^{2+}, Mg^{2+}, Zn^{2+}, Cd^{2+}, Mn^{2+}, Co^{2+}, Ni^{2+}, Hg^{2+}, and Pb^{2+} as their perchlorate salts (Table 4). In this context, DPV[43] studies of ferrocenyl thiazoles **3** and **9** indicate that both receptors behave as selective electrochemical sensors for Hg^{2+}, eliciting the same response: the appearance of a new redox peak, anodically shifted from the original ferrocene potential in the free ligand. However, the magnitudes of these redox shifts were different depending on the position of the ring to which the ferrocene unit is bonded. The magnitude of $\Delta E_{1/2}$ is 100 mV for **3**, and 140 mV for **9**, which bears the ferrocene moiety appended at 5 and 2 positions of the thiazole ring, respectively. In contrast, addition of Ca^{2+}, Mg^{2+}, Zn^{2+}, Cd^{2+}, Mn^{2+}, Co^{2+}, Ni^{2+}, and Pb^{2+} ions to these ligands do not promote any significant change in the corresponding electrochemical responses. Similar voltammetric titrations were also carried out by adding the above-mentioned cations to a solution of ligands **7**, **11**, and **14**. Unfortunately, a dramatic decrease in the sensing properties of these receptors was evidenced, and no useful responses could be obtained.

Interestingly, ligand **5** possessing two ferrocene units linked to the 2 and 5 positions of the thiazole ring gives rise to noticeable metal ion binding processes upon addition of Zn^{2+}, Cd^{2+}, Ni^{2+}, and Pb^{2+} cations. Whereas no perturbation of the voltammograms was observed upon addition of Ca^{2+}, Mg^{2+}, Mn^{2+}, and Co^2 even in a large excess, a significant modification was observed for the first oxidation peak upon addition of Zn^{2+}, Cd^{2+}, Ni^{2+}, and Pb^{2+} metal ions. In contrast, the second oxidation peak was apparently not perturbed on the addition of these cations, as happened for the protonation studies. Again, this suggests that the complex is disrupted after the first monoelectronic oxidation of the complex and the second oxidation really takes place on the uncomplexed mono-oxidized species $\mathbf{5}^{\bullet+}$ (Figure 5).

Previous studies on ferrocene-based ligands have shown that their characteristic low-energy (LE) bands in the absorption spectra are perturbed by complexation.[44] Therefore, the metal recognition properties of both mono- and bis-thiazolyl ferrocene ligands toward Ca^{2+}, Mg^{2+}, Zn^{2+}, Cd^{2+},

(42) Plenio, H.; Yang, J.; Diodone, R.; Huinze, J. *Inorg. Chem.* **1994**, *33*, 4098−4104.

(43) DPV technique has been employed to obtain well-resolved potential information, while the individual redox process are poorly resolved in the CV experiments in individual $E_{1/2}$ potential can not be accurately extracted easily from this data. See: Serr, B. R.; Andersen, K. A.; Elliot, C. M.; Anderson, O. P. *Inorg. Chem.* **1988**, *27*, 4499−4504.

(44) (a) Marder, S. R.; Perry, J. W.; Tiemann, B. G. *Organometallics* **1991**, *10*, 1896−1901. (b) Coe, B. J.; Jones, C. J.; McCleverty, J. A.; Bloor, D.; Cross, G. J. *J. Organomet. Chem.* **1994**, *464*, 225−232. (c) Müller, T. J.; Netz, A.; Ansorge, M. *Organometallics* **1999**, *18*, 5066−5074.

Table 4. Relevant Physicochemical Data of the Ligand/Metal Complexes Formed

compd		Cd^{2+}	Zn^{2+}	Hg^{2+}	Ni^{2+}	Pb^{2+}
3	λ^a			337 (13320), 514 (1930)		337 (13200), 514 (1920)
	$\Delta\lambda^b$			65		65
	log $K_{as}{}^c$			3.58 ± 0.11		3.58 ± 0.13
	L/M^d			1/1		1/1
	Ep^e			0.62		
5	λ^a	337 (11564), 523 (3236)	336 (11484), 518 (2989)	339 (12024), 525 (3983)	338 (12109), 524 (3483)	340 (11970) 525 (3950)
	$\Delta\lambda^b$	66	61	68	67	68
	log $K_{as}{}^c$	3.58 ± 0.11	6.43 ± 0.54	6.24 ± 0.57	6.28 ± 0.55	6.50 ± 0.40
	L/M^d	1/1	2/1	2/1	2/1	2/1
	Ep^e	**0.63**	**0.63**	**0.67**	**0.63**	**0.65**
7	λ^a	393 (10790), 565 (4250)	395 (10680), 571 (3958)	401 (10040), 514 (2720), 595 (2740)	393 (10856), 571 (4256)	400 (10120) 513 (2730), 595 (2660)
	$\Delta\lambda^b$	79	85	109	85	109
	log $K_{as}{}^c$	6.33 ± 0.43	6.21 ± 0.39	5.29 ± 0.32	6.40 ± 0.45	5.00 ± 0.27
	L/M^d	2/1	2/1	1/1	2/1	1/1
	Ep^e					
9	λ^a	333 (12320), 515 (1400)	342 (13440), 525 (2380)	343 (13380), 526 (2460)	333 (12870), 515 (1520)	340 (13400) 523 (2470)
	$\Delta\lambda^b$	56	66	67	66	64
	log $K_{as}{}^c$	7.22 ± 0.34	6.23 ± 0.35	7.38 ± 0.37	7.11 ± 0.35	7.30 ± 0.30
	L/M^d	2/1	1/1	2/1	2/1	2/1
	Ep^e			0.71		
11	λ^a	329 (30420), 476 (2120)	323 (28350), 489 (1750)	332 (23730), 516 (1620)	322 (28810), 508 (1710)	333 (23900) 514 (1590)
	$\Delta\lambda^b$	7	20	47	39	45
	log $K_{as}{}^c$	3.65 ± 0.11	4.56 ± 0.35	4.47 ± 0.41	4.93 ± 0.37	4.30 ± 0.36
	L/M^d	1/2	1/1	1/2	1/1	1/2
	Ep^e					
14	λ^a			330 (21740), 485 (2820)		331 (21500), 485 (2790)
	$\Delta\lambda^b$			26		26
	log $K_{as}{}^c$			3.25 ± 0.13		3.10 ± 0.09
	L/M^d			1/2		1/2
	Ep^e					

^{a} λ_{max} /nm (ϵ [dm^3 mol^{-1} cm^{-1}]). ^{b} Red-shift of the LE band upon metal complexation ($\Delta\lambda = \lambda_{complexed} - \lambda_{freeligand}$). ^{c} Association constant determined by Specfit/32 Global Analysis System. ^{d} Stoichiometry of the complex formed (ligand/metal). ^{e} Volts vs SCE, Pt working electrode, CH_2Cl_2 containing 1 M [(*n*-Bu)$_4$N]ClO$_4$, 20 °C.

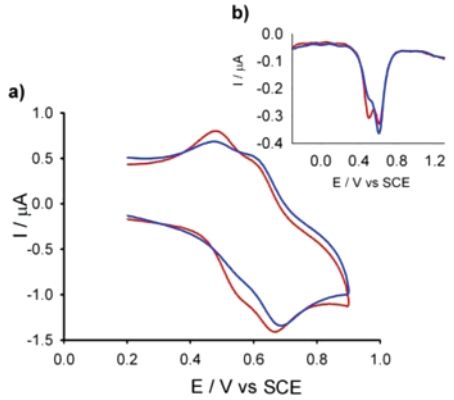

Figure 5. (a) Evolution of cyclic voltammogram of free ligand **5** (1 mM) (red) until the formation of the complex **5**·Cd^{2+} (blue) in CH_2Cl_2/CH_3CN (3/2) using [(*n*-Bu)$_4$N]ClO$_4$ as supporting electrolyte scanned at 100 mV s^{-1}. (b, inset) Evolution of DPV of free ligand **5** (1 mM) (red) until the formation of the complex **5**·Cd^{2+} (blue) in CH_2Cl_2/CH_3CN (3/2) using [(*n*-Bu)$_4$N]ClO$_4$ as supporting electrolyte scanned at 100 mV s^{-1}.

Mn^{2+}, Co^{2+}, Ni^{2+}, Hg^{2+}, and Pb^{2+} ions were also evaluated by UV−vis spectroscopy (Table 4). Titration experiments for dichloromethane solutions of ligand ($c = 1 \times 10^{-4}$ M) and the corresponding ions were performed and analyzed quantitatively.[45] It is worth mentioning that no changes were observed in the UV−vis spectra of any of these ligands upon addition of 1 equiv of Ca^{2+}, Mg^{2+}, Mn^{2+}, and Co^{2+} metal ions. However, from the spectrophotometric behavior of these derivatives upon addition of Zn^{2+}, Cd^{2+}, Ni^{2+}, Hg^{2+}, and Pb^{2+} ions, it is clear that the binding events are strongly affected by the position of the heterocyclic ring at which the ferrocene nucleus is linked, indicating that shorter distances between the nitrogen donor atom within the heterocyclic ring and the ferrocene unit correspond to smaller selectivity in the recognition properties of the ligand.

For compounds **3** and **14**, in which the ferrocene unit is linked at the 5 position of the thiazole ring, the presence of Hg^{2+} and Pb^{2+} ions induced a red-shift of the LE bands from 449 and 459 nm to 514 and 485 nm, respectively (Table 4), whereas no changes in the UV−vis spectra of these ligands were observed upon addition of an excess of Ca^{2+}, Mg^{2+}, Zn^{2+}, Cd^{2+}, Mn^{2+}, Co^{2+}, and Ni^{2+} ions. In contrast, the UV−vis data obtained by addition of Ca^{2+}, Mg^{2+}, Mn^{2+}, Co^{2+}, Ni^{2+}, Hg^{2+}, and Pb^{2+} ions to the mono- (**5** and **9**) and bis-thiazolyl (**11**) ligands, bearing the ferrocene nucleus attached to the 2 position, revealed that while no changes were detected in the case of Ca^{2+}, Mg^{2+}, Mn^{2+}, and Co^{2+} ions, a red-shift of their LE bands upon addition of Zn^{2+}, Cd^{2+}, Hg^{2+}, Ni^{2+}, and Pb^{2+} ions was observed (Table 4).

Regarding bidentate compound **7**, the addition of Zn^{2+}, Cd^{2+}, and Ni^{2+} metal ions induced a red shift of the LE band by 79−85 nm, whereas the Hg^{2+} and Pb^{2+} metal ions

(45) All titration experiments were analyzed using the computer program Specfit/32 Global Analysis System, 1999−2004, Spectrum Software Associates (SpecSoft@compuserve.com). The equation to be adjusted by nonlinear regression, using the above mentioned software, was the following: $\Delta A/b = \{K_{11}\Delta\epsilon_{HG}[H]_{tot}[G]\}/\{1 + K_{11}[G]\}$, where H = host, G = guest, HG = complex, ΔA = variation in the absorption, b = cell width, K_{11} = association constant for a 1:1 model, and $\Delta\epsilon_{HG}$ = variation of molar absorptivity.

promoted a higher red shift by 109 nm. As it happened for all the series of ferrocenylthiazoles, no significant response was obtained when the divalent cations added were Ca^{2+}, Mg^{2+}, Mn^{2+}, or Co^{2+}.

In those cases where an optical response could be detected, the observation of isosbestic points in the evolution of the UV−vis spectra clearly indicates that clean complexation equilibria take place. It is also worth mentioning that addition of cations (not shown) beyond the point of equivalence for each complex did not cause a significant change in the absorption spectra. Titration analysis data gave the stability constants displayed in Table 4 and confirmed the formation in solution of the reported ligand/metal complex stoichiometries.

A further exciting property of these ligands is that they are not only able to monitor binding but they are also able to behave as actuators through the progressive electrochemical release of the metal cation; that is, the binding constant upon electrochemical oxidation is decreased.

In this context, a spectroelectrochemical study of complex **3**·Hg^{2+}, as a model complex, was carried out. Thus, 1 equiv of $Hg(ClO_4)_2$ was added to a solution of **3** in CH_2Cl_2, with $[(n\text{-}Bu)_4N]PF_6$ (0.15 M) as supporting electrolyte, in order to obtain the complexed **3**·Hg^{2+} species that exhibits an intense purple color. The complex was oxidized at +0.9 V versus $Ag/AgNO_3$ until the complete oxidation was reached and the color of the solution changed from purple to yellow. Afterward, the solution was completely reduced with a potential of −0.1 V versus $Ag/AgNO_3$, and the initial spectrum was fully recovered as well as its purple color. Thus, the free oxidized ligand **3**$^{\bullet+}$ is reduced to **3** which has a huge cation Hg^{2+} binding affinity leading the initial complex **3**·Hg^{2+}. Oxidation of the complex **3**·Hg^{2+} and its subsequent reduction were carried out over several cycles in a chronoamperometric experiment, as shown in Figure 6. After each step, the optical spectrum was recorded, and it was found to be recovered, demonstrating the high degree of reversibility of the complexation/decomplexation process, although in the reduction steps the intensity of the optical spectra recorded decrease slowly, as the working electrode is passivated. This result shows that complex **3** is an electrochemically induced switchable chemosensor.

From the combined voltammetric and optical studies, several trends can be extracted from this study. First, ferrocenylthiazoles linked accross the 5 position of the heteroaromatic ring are selective chemosensors for Hg^{2+} and Pb^{2+} metal ions with the 5-ferrocenylthiazole **3** operating through two channels: optical and redox (Figure 7), whereas 1,1′-bis(thiazolyl)ferrocene **14** only operates as an optical sensor. Second, ferrocenylthiazole **9**, with the ferrocenyl unit linked to the 2 position of the heterocyclic ring, is a selective redox sensor for Hg^{2+} metal ions, and it responds optically to a narrow range of cations, comprising Zn^{2+}, Cd^{2+}, Hg^{2+}, Ni^{2+}, and Pb^{2+}, as the bis(thiazolyl)ferrocene **11** does. Third, bis(ferrocenyl)thiazole **5** is a dual optical and redox sensor for Zn^{2+}, Cd^{2+}, Hg^{2+}, Ni^{2+}, and Pb^{2+}, whereas bis(ferrocenyl) compound **7**, bearing a bis(thiazole) as a bridge, is only a chromogenic sensor for Zn^{2+}, Cd^{2+}, Ni^{2+} (color changes from orange to blue), and Hg^{2+} (color changes from orange to green) (Figure 8). This study also revealed the ability of these ligands to control the trapping and the expulsion of these metal ions by application of an external electrochemical stimulus.

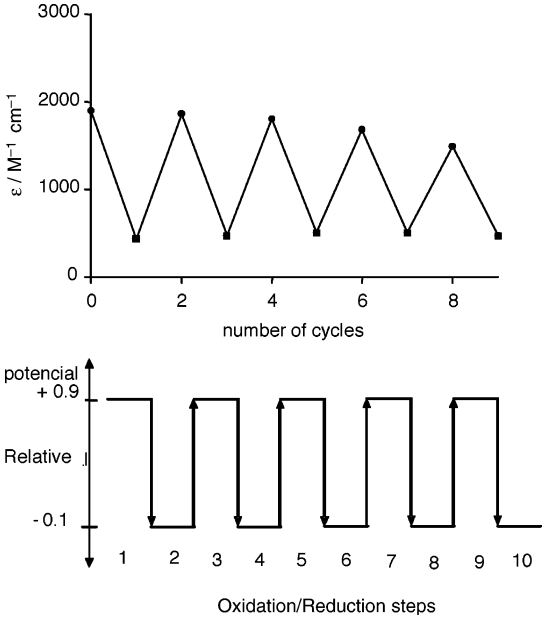

Figure 6. Cyclic stepwise oxidation and reduction of **3**·Hg^{2+} carried out in CH_2Cl_2 with a chronoamperometric technique following the changes by UV−vis−near-IR spectroscopy. Upper: changes observed at a wavelength of 513 nm (reduction) and 863 nm (oxidation). Lower: fixed potentials used in the different steps of cyclic redox experiments.

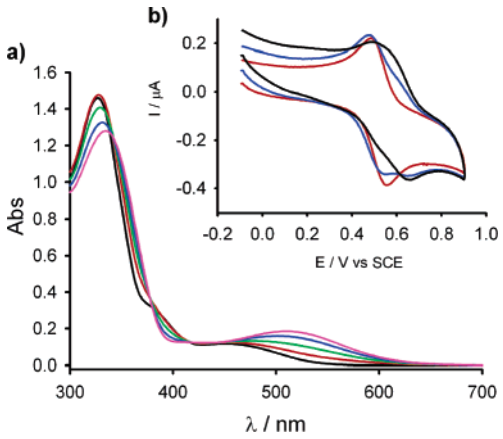

Figure 7. (a) Changes in the absorption spectra of **3** upon addition of increasing amounts of Hg^{2+}. The initial spectrum (black) is that of the free ligand, and the final spectrum (purple) corresponds to the addition of 1 equiv of Hg^{2+}. (b, inset) Cyclic voltammogram of compound **3** (1 mM), in CH_2Cl_2/CH_3CN (3/2) using $[(n\text{-}Bu)_4N]ClO_4$ as supporting electrolyte scanned at 100 mV s^{-1} from −0.1 to 0.95 V (red), after addition of 0.5 equiv of Hg^{2+} (blue) and 1 equiv of Hg^{2+} (black).

Theoretical Calculations. Quantum chemical calculations at the DFT level provided insight concerning the complexation abilities (both in their neutral or oxidized states) toward divalent metal ions of the compounds presented here as well as their electronic structures. Calculations were performed in bisferrocenylthiazoles **5** and **7** and in monoferrocenylthiazoles **3** and **9**, as well as on the recently reported "open-chain" 1,4-bis(ferrocenyl)-2-aza-1,3-butadiene.[8a] The com-

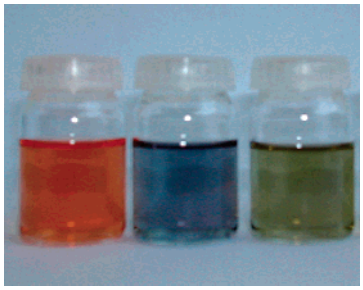

Figure 8. Changes of colors observed upon addition to the free ligand **7** (left), Cd^{2+}, Zn^{2+}, or Ni^{2+} ions (center), and Hg^{2+} (right).

prehensive theoretical study carried out is shown completely in the Supporting Information.

Upon one-electron oxidation, bisferrocenyl thiazole **5** behaves in an unprecedented way, inasmuch as both ferrocene units lose nearly equal amounts of electron density initially, but the unstable radical cation generated undergoes geometrical relaxation with IET from the most oxidized Fc_1 unit (the one closer to the N atom) to the less positively charged Fc_2 unit. This results in a highly positively charged "fully oxidized" Fc_1 unit with an almost "unoxidized" Fc_2 moiety. The second one-electron oxidation takes place again by removing the electron density from Fc_2.

The ion binding properties of ferrocenylthiazole derivatives have also been studied by means of DFT quantum chemical calculations using model systems. A divalent metal perchlorate was complexed with the model ligand L (where L stands for 2-ferrocenylthiazole or 5-ferrocenylthiazole) to give $[L \cdot M]^{2+}$ and two perchlorate anions, with every species being considered as noninteracting, and their energies were computed in dichloromethane as solvent (see the Computational Procedures subsection).

From the studies carried out, several conclusions can be extracted. First, the ferrocenyl substitution at the 2 position of thiazole leads to more stable complexes (involving Fe and N as donor atoms) than at the 5 position with all studied divalent metal ions. Except for the complexation of Cd^{2+}, the Fe,N and Fe,S binding modes are the best combinations of donor sites for 2- and 5-ferrocenylthiazoles, respectively. Thus, in bisferrocenyl thiazole **5** metal complexation is expected to occur involving Fe_1 and the heterocyclic N atom. Second, with both model ligands the most stable complexes were found with mercury (see Figure 9). Indeed, the complexation of Hg^{2+} by 5-ferrocenyl thiazole is the only thermodynamically favored reaction at the working level of theory. The relative difference in complexation energy with other ions (31.24, 43.86, 74.53, 78.09, and 91.20 kcal/mol for Cd^{2+}, Zn^{2+} Ni^{2+}, Mg^{2+}, and Pb^{2+}, respectively) is large enough to account for a high selectivity. These differences are much lower in the case of 2-ferrocenylthiazole ligand (16.53, 22.27, 60.82, 55.66, and 81.12 kcal/mol for Cd^{2+}, Zn^{2+} Ni^{2+}, Mg^{2+}, and Pb^{2+}, respectively), indicating therefore a lower selectivity. Third, minima corresponding to the Fe,S binding mode were also found for 2-ferrocenylthiazole (except with Ni^{2+} and Pb^{2+} which evolves to the Fe,N complexation mode), with similar energies to those of 5-ferrocenylthiazole. Additional minima involve the outer

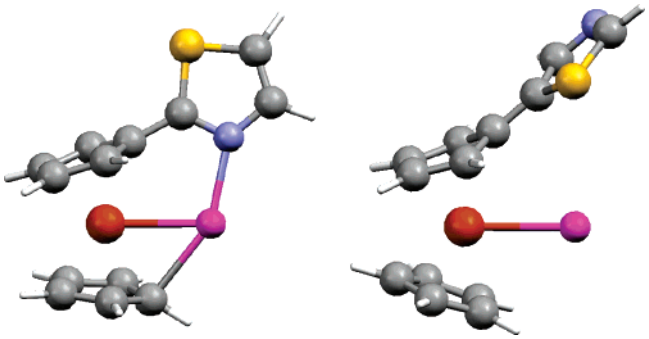

Figure 9. Calculated (method A) structures for the most stable complexes formed between Hg^{2+} and 2-ferrocenylthiazole (left) and 5-ferrocenylthiazole (right).

side of Cp_1 as η^5 donor site (except for Hg^{2+}), corresponding to the most stable complexes of Cd^{2+} for the former ligand.

Summary

The synthesis, optical and electrochemical properties, and X-ray characterization of two thiazole ring systems capped with two ferrocenyl groups (**5** and **7**) and their model compounds with only one ferrocenyl, either at 2 or 5 position of the mono- or bis-thiazolyl ligands (**3**, **9**, **11**, and **14**), are presented. These ferrocenyl heteroaromatic ligands could serve as important models for the investigation of intramolecular electron transfer and for metal recognition processes. Bisferrocenyl thiazole **5** forms the mixed-valence species $\mathbf{5}^{\bullet+}$ by partial oxidation which, interestingly, shows an IET phenomenon because of the electronic coupling between the two ferrocene units which is rather unusual for heteroaromatic ring systems capped by ferrocenyl groups. Monoferrocenyl thiazoles in their oxidized forms display absorption bands assigned to thiazole $\rightarrow Fe^{III}$ LMCT transitions. On the other hand, the compounds studied exhibit interesting ion-sensing properties which show high selectivity for divalent metal ions giving responses through one or two channels. Thus, ferrocenylthiazoles linked accross the 5 position of the heteroaromatic ring are selective chemosensors for Hg^{2+} and Pb^{2+} metal ions with 5-ferrocenylthiazole **3** operating through two optical and redox channels whereas the 1,1′-bis(thiazolyl)ferrocene **14** operates as an optical sensor only. Compound **3** also exhibited a selective Hg^{2+} induced complexation/decomplexation type of signaling pattern that can be used for the construction of more elaborate supramolecular switching systems. Moreover, ferrocenylthiazole **9**, in which the heterocyclic ring and the ferrocene group are linked across the 2 position, is a selective redox sensor for Hg^{2+} metal ions, and it responds optically, as bis(thiazolyl)ferrocene **11** does, to a narrow range of cations, comprising Zn^{2+}, Cd^{2+}, Mn^{2+}, Co^{2+}, Hg^{2+}, Ni^{2+}, and Pb^{2+}. Finally, bis(ferrocenyl)thiazole **5** is a dual optical and redox sensor for Zn^{2+}, Cd^{2+}, Mn^{2+}, Co^{2+}, Hg^{2+}, Ni^{2+}, and Pb^{2+}, whereas bis(ferrocenyl) compound **7**, bearing a bis(thiazole) as a bridge, is only a chromogenic sensor for Zn^{2+}, Cd^{2+}, Mn^{2+}, Co^{2+}, and Ni^{2+}, promoting a color change from orange to blue, and Hg^{2+} and Pb^{2+}, where a change of color from

orange to green is observed. The experimental data and conclusions about both the electronic and ion-sensing properties are supported by DFT computations and show, in addition, an unprecedented intramolecular electron-transfer reorganization after the first one-electron oxidation of compound **5**.

Acknowledgment. We gratefully acknowledge the grants from Ministerio de Educación y Ciencia (MEC), Spain, CTQ2004-02201 and MAT2003-04699, and "Eje C-Consolider" EMOCIONa (CTQ2006-06333/BQU), from Generalitat de Catalunya 2005 SGR-00591 and from Fundación Séneca (CARM) 02970/PI/05. A.C. also thanks Ministerio de Eucación y Ciencia for a predoctoral grant. D.C. is grateful to Ministerio de Educación y Ciencia and Universidad de Murcia for a Ramón y Cajal contract. The authors also thank David B. Amabilino (ICMAB, CSIC) for his corrections and suggestions for this work.

Supporting Information Available: Relevant spectroscopic data for the new synthesized compounds; crystal data and details of data collection and structure refinement of compounds **3**, **5**, **11**, and **14**; crystal packing of neutral compounds **3**, **5**, **11**, and **14**; CV and DPV of compounds **3**, **5**, **9**, and **14** before and after addition of metal cations; evolution of the UV−near-IR data during the course of the oxidation of compound **3**; variation of the UV−vis data of **3**, **5**, **7**, **9**, **11**, and **14** upon addition of different metal cations; EPR data of some compounds; comprehensive theoretical study of the oxidative event in ferrocenylthiazoles and their complexating behavior. This material is available free of charge via the Internet at http://pubs.acs.org.

IC061803B